International Journal of Structural Stability and Dynamics
(2027) 2750012 (27 pages)

DOI: 10.1142/S021945542750012X

Investigation of Nonlinear Dynamic Stability and Phase/Group Velocity in 3D Functionally Graded Skew Nanoplates for Concrete Building Applications

Jianfeng Li*,¶, Mohammed El-Meligy†,‡ and Ahmed Ahmed Ibrahim§

*College of Civil and Transportation Engineering
Shenzhen University, Shenzhen 518060, P. R. China

†Jadara University Research Center
Jadara University, P.O. Box 733, Irbid, Jordan

‡Applied Science Research Center
Applied Science Private University, Amman, Jordan

§Department of Physics and Astronomy, College of Science
King Saud University, P.O. Box 2455, Riyadh 11451, Saudi Arabia

¶1479205116@qq.com

Received 7 June 2025
Accepted 4 August 2025
Published 3 October 2025

This study presents a comprehensive investigation of nonlinear wave propagation and the phase–group velocity characteristics in three-dimensional functionally graded material (3D-FGM) skew nanoplates, with a focus on concrete building applications. The hyperbolic shear deformation theory of higher order is employed to account for the geometrical nonlinear response using Von Karman strain assumption and nonlocal strain gradient theory (NSGT) capturing the nanoscale size dependency. The nonlinear governing equations of motion that describe the dynamic behavior under wave excitation are derived using Hamilton's principle. Because of the complexity of the system, obtaining an exact analytical solution is difficult; therefore, an efficient iterative finite element technique is formulated. More specifically, isoparametric-to-standard element conversion in the framework allows computational efficiency while minimizing inaccuracies. The model is validated for some of these cases against the literature, where available, confirming the ability of this methodology to capture wave phenomena. The effects of gradient index, nanoplate skewness, nonlocal parameters, and thickness-to-length ratios on the wave characteristics are also discussed extensively. The results have shown pronounced dispersion and shifts in mode shapes, which are affected by material gradation, nonlocal effects. These results are important for wave-based sensing, nondestructive evaluation, and structural health monitoring of advanced nanostructures. The model proposed here shows an ability to capture complex waves for high-angle boundaries as well as those that

¶Corresponding author.

demonstrate omega-squared behavior, thus validating the suitability of the approach for physics-driven materials with complex wave propagation.

Keywords: Nonlinear wave propagation; 3D-FGM; phase and group velocity; nonlocal strain gradient theory; concrete building applications; higher-order hyperbolic shear deformation theory.

1. Introduction

Functionally graded materials (FGMs) are crucial for engineering as they offer tailored properties that can be optimized for specific applications, improving material performance.[1] By varying the composition and microstructure gradually over the material's volume, FGMs enhance strength, durability, and resistance to thermal, mechanical, and environmental stresses.[2] This property gradient allows engineers to design components that are more efficient, lightweight, and resistant to failure under extreme conditions.[3] FGMs are particularly valuable in aerospace, automotive, and civil engineering, where materials are subjected to high-temperature gradients, mechanical loading, and wear.[4] As the demand for high-performance materials increases, FGMs provide a versatile solution to meet the complex requirements of modern engineering challenges.[5]

Nonlinear wave mechanics is essential for engineers because it provides a deeper understanding of wave behaviors in complex materials and structures, which are often subjected to extreme conditions.[6] Unlike linear wave theory, nonlinear wave mechanics accounts for phenomena such as wave amplification, shock formation, and frequency shifts, which are critical in real-world applications.[7] Engineers can apply nonlinear wave principles to design more efficient systems for vibration control, acoustics, and signal processing in industries like aerospace, automotive, and civil engineering.[8] The study of nonlinear waves also enables the prediction of material failure, fatigue, and the dynamic response of structures under nonlinear loading conditions.[9] As engineering challenges become more complex, incorporating nonlinear wave mechanics ensures more accurate designs and enhanced safety and performance.[10]

Stability analysis is a fundamental aspect of engineering that ensures the safety, reliability, and performance of structures under various loading conditions.[11] It involves evaluating how structures respond to external forces and predicting the point at which they may lose equilibrium, leading to failure or excessive deformation.[12] This analysis is crucial in identifying potential failure modes such as buckling, vibration instability, or collapse, which can result in catastrophic consequences.[13] Engineers rely on stability analysis to design structures that not only meet safety standards but also optimize material use, reduce costs, and enhance longevity.[14] By considering factors like load distribution, boundary conditions, and material properties, stability analysis helps engineers understand the dynamic behavior of

structures in both static and dynamic environments.[15] The application of stability principles extends across various fields, including civil, mechanical, aerospace, and materials engineering.[16] In modern design, particularly with advanced materials like composites and functionally graded materials, stability analysis is even more critical due to complex interactions between various physical factors, such as temperature, moisture, and electrical fields.[17] Overall, stability analysis serves as a cornerstone of engineering design, ensuring that structures can perform safely and efficiently throughout their service life.[18] Stability analysis also plays a crucial role in the development of innovative structural systems, enabling engineers to push the boundaries of design while maintaining safety and functionality.[19] Additionally, with the increasing complexity of modern engineering materials and structures, advanced stability analysis techniques, including nonlinear and dynamic approaches, are becoming essential to accurately predict behavior under extreme conditions.[20]

Nanostructures play a critical role in enhancing the performance and durability of concrete in building applications.[19]

In this work, for the first time, this paper investigates nonlinear wave propagation and the phase–group velocity behavior in three-dimensional functionally graded skew nanoplates, specifically for concrete building applications. Utilizing a higher-order hyperbolic shear deformation theory (HHSDT), the structural formulation accounts for Von Karman's geometrical nonlinearity to capture moderate to large deformations and integrates the nonlocal strain gradient theory (NSGT) to incorporate nanoscale effects. The governing equations of motion are derived using Hamilton's principle and discretized through a refined finite element method. To enhance computational accuracy and stability, isoparametric elements are transformed into standard elements. Due to the analytical intractability of the nonlinear system, an efficient iterative numerical strategy is developed. The effects of material gradation, nanoplate skewness, length-scale parameters, and thickness variations are thoroughly examined. The results reveal that nonlocal and gradient effects significantly influence wave propagation behavior, particularly at higher frequencies where nonlinearity and nanoscale interactions are most prominent. This study offers valuable insights for the design and dynamic analysis of advanced FGM nanostructures, with implications for structural health monitoring, ultrasonic sensing, and the development of next-generation concrete-based nanoengineered devices. The proposed framework demonstrates robust predictive capabilities for wave mechanics in functionally graded nanoplates, capturing both geometric and material nonlinearities. The novelties of this work can be divided into four fields: (1) First investigation of nonlinear wave propagation in 3D FGM skew nanoplates for concrete applications. (2) Integration of NSGT with higher-order shear deformation for nanoscale effects of skew nanoplate. (3) Refined finite element method with isoparametric-to-standard element conversion enhances computational accuracy and stability. (4) Comprehensive analysis of

material gradation, nanoplate skewness, and nanoscale effects on wave propagation.

2. Effective Material Properties

2.1. *Three-directional functionally graded materials (3D-FGM)*

As the name suggests, FGM exhibit changes in properties across their structure. These property changes are typically described using mathematical functions. Among the various options, the power-law function is the most widely used, particularly within a Cartesian coordinate framework.[21]

$$\begin{aligned} E(x,y,z) &= E_m + (E_c - E_m)\left(\frac{x}{a}\right)^{n_x}\left(\frac{y}{b}\right)^{n_y}\left(0.5+\frac{z}{h}\right)^{n_z}, \\ v(x,y,z) &= v_m + (v_c - v_m)\left(\frac{x}{a}\right)^{n_x}\left(\frac{y}{b}\right)^{n_y}\left(0.5+\frac{z}{h}\right)^{n_z}, \\ \rho(x,y,z) &= \rho_m + (\rho_c - \rho_m)\left(\frac{x}{a}\right)^{n_x}\left(\frac{y}{b}\right)^{n_y}\left(0.5+\frac{z}{h}\right)^{n_z}. \end{aligned} \tag{1}$$

Assigning specific values to the power indices n_x, n_y and n_z effectively removes material gradation along the corresponding directions. The elastic characteristics of the two constituent materials forming the functionally graded composite used in this analysis are listed in Table 1. Given that the study focuses on the dynamic response of the structure, the mass densities of the materials are also included in the table. The functionally graded material in question is a metal-based composite, featuring a nonuniform distribution of aluminum oxide (Al_2O_3) concrete within a steel fiber-reinforced concrete.[22,23]

2.2. *Mathematical modeling*

This paper includes the key assumptions and modifications made in the modeling process. Specifically, Von Karman's strain assumptions are used to model geometrical nonlinearity, while the NSGT captures nanoscale size-dependent effects. A continuous material distribution in the thickness direction is assumed to model the three-dimensional functionally graded material (3D-FGM). Additionally, the harmonic wave excitation is applied at the surface to study wave propagation. These

Table 1. The material properties of the 3D FGMs rectangular plate.[22,23]

Ceramic (Al_2O_3 concrete)	Metal (Steel fiber-reinforced concrete)
$E_c = 348.43 \times 10^9$ [pa]	$E_m = 235 \times 10^9$ [pa]
$v_c = 0.2400$	$v_m = 0.2700$
$\rho_c = 2\ 170\ \left[\frac{\text{Kg}}{\text{m}^3}\right]$	$\rho_m = 2\ 800\ \left[\frac{\text{Kg}}{\text{m}^3}\right]$

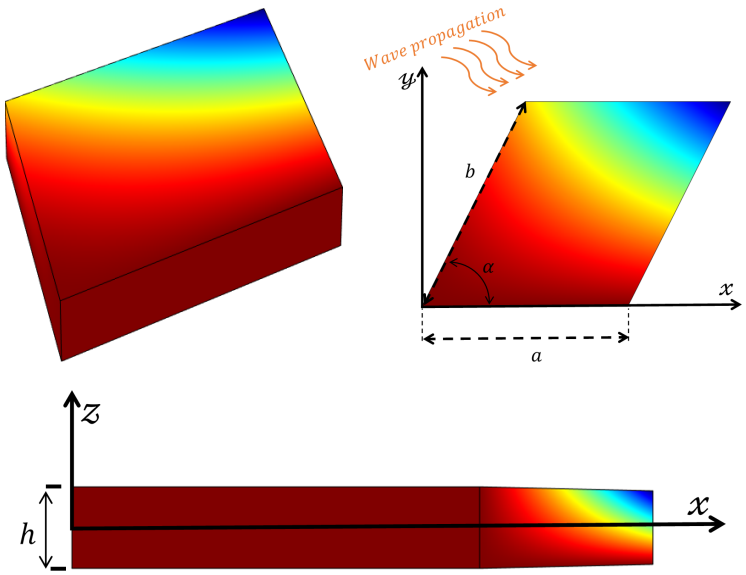

Fig. 1. Schematic representation of a 3D FGM nanoplate.

assumptions and modifications are necessary to balance computational efficiency with accuracy in modeling wave dynamics. Consider a skewed plate whose geometric configuration is illustrated in Fig. 1, referenced within a Cartesian coordinate framework.

2.3. *The nonlocal strain gradient theory*

Traditional elasticity theory, which relies on local material point assumptions, falls short in describing the size-dependent responses observed in micro and nanoscale structures. To address these limitations, advanced frameworks such as nonlocal elasticity and strain gradient theories have been introduced, offering better insight into scale-dependent material behavior. Each of these models is tailored to specific scales and application contexts. To leverage the advantages of both approaches, a unified framework known as the NSGT has been developed and applied in various studies. The fundamental formulation of this theory is presented below[51]:

$$\sigma_{ij} - \mu^2 \sigma_{ij,mm} = \mathcal{C}_{ijkl}(\varepsilon_{kl} - l^2 \varepsilon_{kl,mm}). \tag{2}$$

In addition to the traditional stress tensor σ_{ij}, strain tensor ϵ_{ij}, and elasticity tensor C_{ijkl} defined in classical linear elasticity, the NSGT introduces two additional material-specific parameters. These are the nonlocal coefficient μ and the length

scale parameter l, which accounts for strain gradient effects. The Laplacian operator in the formulation is denoted using repeated indices as $\boxdot_{mm}$. By individually activating either the nonlocal parameter or the gradient length scale parameter, one can retrieve the original nonclassical models of nonlocal elasticity and strain gradient theory, respectively.

$$\begin{aligned}(1-\mu^2\nabla^2)\sigma_{ij} &= t_{ij},\\ \sigma_{ij} &= \mathcal{C}_{ijkl}(\varepsilon_{ij}-l^2\varepsilon_{ij,mm}),\end{aligned} \tag{3}$$

where $\nabla^2 = \frac{\partial^2}{\partial x^2} + \frac{\partial^2}{\partial y^2}$ represents the Laplacian operator.

2.4. *Displacement field and strains*

In this work, the displacement field of the sandwich plate is characterized using the HHSDT, as detailed in the following equation[24]:

$$\begin{aligned}u(x,y,z,t) &= u_0(x,y,t) + \mathcal{F}(z)u_1(x,y,t) + \mathcal{G}(z)u_2(x,y,t),\\ v(x,y,z,t) &= v_0(x,y,t) + \mathcal{F}(z)v_1(x,y,t) + \mathcal{G}(z)v_2(x,y,t),\\ w(x,y,z,t) &= w_0(x,y,t).\end{aligned} \tag{4}$$

Terms $u_0, v_0, w_0, u_1, v_1, u_2$, and v_2 represent seven unknown displacement functions defined on the mid-surface of the plate, while $\mathcal{F}(z)$, $\mathcal{G}(z)$ serve as the thickness-dependent shape functions. Various forms of these shape functions have been proposed in previous research. In the present study, newly developed hyperbolic expressions for $\mathcal{F}(z)$ and $\mathcal{G}(z)$ are utilized and are formulated as follows[24]:

$$\begin{aligned}\mathcal{F}(z) &= \Omega\cdot\tanh\left(\frac{z}{h}\right) + \Phi\cdot\sinh\left(\frac{\pi z}{h}\right),\\ \mathcal{G}(z) &= z - \Omega\cdot\tanh\left(\frac{z}{h}\right) + \Phi\cdot\sinh\left(\frac{\pi z}{h}\right),\end{aligned} \tag{5}$$

where

$$\begin{aligned}\Omega &= \frac{5h\cosh\left(\frac{\pi}{2}\right)}{4\left[\tanh^2\left(\frac{1}{2}\right)+\cosh\left(\frac{\pi}{2}\right)-1\right]},\\ \Phi &= \frac{5h\left[\tanh^2\left(\frac{1}{2}\right)-1\right]}{4\pi\left[\tanh^2\left(\frac{1}{2}\right)+\cosh\left(\frac{\pi}{2}\right)-1\right]}.\end{aligned} \tag{6}$$

The strain fields of the plate are as follows:

$$\begin{aligned}\boldsymbol{\varepsilon} &= \boldsymbol{\varepsilon}^0 + \mathcal{F}\boldsymbol{\varepsilon}^1 + \mathcal{G}\boldsymbol{\varepsilon}^2,\\ \boldsymbol{\gamma} &= \mathcal{F}'\boldsymbol{\gamma}_1 + \mathcal{G}'\boldsymbol{\gamma}_2 + \boldsymbol{\gamma}_3,\end{aligned} \tag{7}$$

where

$$\boldsymbol{\varepsilon}^0 = \begin{Bmatrix} u_{0,x} + 0.5(w_{0,x})^2 \\ v_{0,y} + 0.5(w_{0,y})^2 \\ u_{0,y} + v_{0,x} + w_{0,x}w_{0,y} \end{Bmatrix}, \quad \boldsymbol{\varepsilon}^1 = \begin{Bmatrix} u_{1,x} \\ v_{1,y} \\ u_{1,y} + v_{1,x} \end{Bmatrix}, \quad \boldsymbol{\varepsilon}^2 = \begin{Bmatrix} u_{2,x} \\ v_{2,y} \\ u_{2,y} + v_{2,x} \end{Bmatrix},$$

$$\boldsymbol{\gamma}_1 = \begin{Bmatrix} \gamma_1^u \\ \gamma_1^v \end{Bmatrix} = \begin{Bmatrix} u_1 \\ v_1 \end{Bmatrix}, \quad \boldsymbol{\gamma}_2 = \begin{Bmatrix} \gamma_2^u \\ \gamma_2^v \end{Bmatrix} = \begin{Bmatrix} u_2 \\ v_2 \end{Bmatrix}, \quad \boldsymbol{\gamma}_3 = \begin{Bmatrix} \gamma_3^u \\ \gamma_3^v \end{Bmatrix} = \begin{Bmatrix} w_{0,x} \\ w_{0,y} \end{Bmatrix}. \tag{8}$$

The linear constitutive relations of the plates are as follows:

$$\boldsymbol{\sigma} = \boldsymbol{D}\boldsymbol{\varepsilon}, \quad \boldsymbol{\tau} = \boldsymbol{D}_s\boldsymbol{\gamma}, \tag{9}$$

where

$$\begin{aligned} \boldsymbol{\sigma} &= \begin{Bmatrix} \sigma_x & \sigma_y & \tau_{xy} \end{Bmatrix}^T, \quad \boldsymbol{\tau} = \begin{Bmatrix} \tau_{xz} & \tau_{yz} \end{Bmatrix}^T, \\ \boldsymbol{D} &= \begin{bmatrix} \mathcal{C}_{11} & \mathcal{C}_{12} & 0 \\ \mathcal{C}_{12} & \mathcal{C}_{22} & 0 \\ 0 & 0 & \mathcal{C}_{66} \end{bmatrix}, \quad \boldsymbol{D}_s = \begin{bmatrix} \mathcal{C}_{55} & 0 \\ 0 & \mathcal{C}_{44} \end{bmatrix}, \\ \mathcal{C}_{11} &= \mathcal{C}_{22} = \frac{E(x,y,z)}{1-(v(x,y,z))^2}, \quad \mathcal{C}_{12} = v(x,y,z)\mathcal{C}_{11}, \\ \mathcal{C}_{44} &= \mathcal{C}_{55} = \mathcal{C}_{66} = \frac{E(x,y,z)}{2(1+v(x,y,z))}. \end{aligned} \tag{10}$$

In this context, $E(z)$ represents Young's modulus, while ν denotes Poisson's ratio. It is important to note that Poisson's ratio is considered constant and uniform for all materials involved. Additionally, the time derivatives of the strain components are included in the constitutive relations, leading to the final governing equations expressed as follows:

$$\begin{aligned} \left(1-\mu^2\nabla^2\right)\sigma_{xx} &= (1-l^2\nabla^2)(\mathcal{C}_{11}\varepsilon_{xx} + \mathcal{C}_{12}\varepsilon_{yy}), \\ \left(1-\mu^2\nabla^2\right)\sigma_{yy} &= (1-l^2\nabla^2)(\mathcal{C}_{12}\varepsilon_{xx} + \mathcal{C}_{22}\varepsilon_{yy}), \\ (1-\mu^2\nabla^2)\tau_{yz} &= (1-l^2\nabla^2)(\mathcal{C}_{44c}\gamma_{yz}), \\ (1-\mu^2\nabla^2)\tau_{xz} &= (1-l^2\nabla^2)(\mathcal{C}_{55c}\gamma_{xz}), \\ (1-\mu^2\nabla^2)\tau_{xy} &= (1-l^2\nabla^2)(\mathcal{C}_{66c}\gamma_{xy}). \end{aligned} \tag{11}$$

2.5. *Hamilton's principle*

The governing equations are obtained through the application of Hamilton's principle, which is expressed in the expanded form below for this specific case[25]:

$$\int_0^t (\delta\Pi - \delta T)\mathrm{d}t = 0. \tag{12}$$

The change in strain energy for the present study is expressed as follows:

$$\delta\Pi = \int_V (\sigma_i \delta E_i + \tau_{ij}\delta\gamma_{ij})\,\mathrm{d}V = \int_V [\sigma_{xx}\delta\varepsilon_{xx} + \sigma_{yy}\delta\varepsilon_{yy} + \tau_{yz}\delta\gamma_{yz} + \tau_{xz}\delta\gamma_{xz} + \tau_{xy}\delta\gamma_{xy}]\mathrm{d}V. \tag{13}$$

The change in kinetic energy for the current analysis is represented as follows:

$$\delta T = \int_V \left\{ \rho(z) \left\{ \left(\frac{\partial u}{\partial t}\frac{\partial \delta u}{\partial t} + \frac{\partial v}{\partial t}\frac{\partial \delta v}{\partial t} + \frac{\partial w}{\partial t}\frac{\partial \delta w}{\partial t} \right) \right\} \right\} \mathrm{d}V. \tag{14}$$

By inserting $\delta\Pi$, and δT into Eq. (12), performing integration across the thickness, applying integration by parts with respect to x and y, and grouping the coefficients of δu_0, δu_1, δu_2, δv_0, δv_1, v_2, and δw_0, the resulting governing equations are derived as follows:

$$\delta u_0 : \frac{\partial \mathcal{N}_{xx}}{\partial x} + \frac{\partial \mathcal{N}_{xy}}{\partial y} - \mathcal{I}_0^{u_0}\ddot{u}_0 - \mathcal{I}_1^{u_0}\ddot{u}_1 - \mathcal{I}_2^{u_0}\ddot{u}_2 = 0, \tag{15a}$$

$$\delta v_0 : \frac{\partial \mathcal{N}_{xy}}{\partial x} + \frac{\partial \mathcal{N}_{yy}}{\partial y} - \mathcal{I}_0^{v_0}\ddot{v}_0 - \mathcal{I}_1^{v_0}\ddot{v}_1 - \mathcal{I}_2^{v_0}\ddot{v}_2 = 0, \tag{15b}$$

$$\delta w_0 : \frac{\partial \mathcal{N}_{xz}}{\partial x} + \frac{\partial \mathcal{N}_{yz}}{\partial y} + \frac{\partial}{\partial x}\left(\mathcal{N}_{xx}\frac{\partial w_0}{\partial x}\right) + \frac{\partial}{\partial y}\left(\mathcal{N}_{yy}\frac{\partial w_0}{\partial y}\right) + \frac{\partial}{\partial x}\left(\mathcal{N}_{xy}\frac{\partial w_0}{\partial y}\right) + \frac{\partial}{\partial y}\left(\mathcal{N}_{xy}\frac{\partial w_0}{\partial x}\right) - \mathcal{I}_0^{w_0}\ddot{w}_0 = 0, \tag{15c}$$

$$\delta u_1 : \frac{\partial \mathcal{M}_{xx}}{\partial x} + \frac{\partial \mathcal{M}_{xy}}{\partial y} - \mathcal{M}_{xz} - \mathcal{I}_0^{u_1}\ddot{u}_0 - \mathcal{I}_1^{u_1}\ddot{u}_1 - \mathcal{I}_2^{u_1}\ddot{u}_2 = 0, \tag{15d}$$

$$\delta v_1 : \frac{\partial \mathcal{M}_{xy}}{\partial x} + \frac{\partial \mathcal{M}_{yy}}{\partial y} - \mathcal{M}_{yz} - \mathcal{I}_0^{v_1}\ddot{v}_0 - \mathcal{I}_1^{v_1}\ddot{v}_1 - \mathcal{I}_2^{v_1}\ddot{v}_2 = 0, \tag{15e}$$

$$\delta u_2 : \frac{\partial \mathcal{P}_{xx}}{\partial x} + \frac{\partial \mathcal{P}_{xy}}{\partial y} - \mathcal{P}_{xz} - \mathcal{I}_0^{u_2}\ddot{u}_0 - \mathcal{I}_1^{u_2}\ddot{u}_1 - \mathcal{I}_2^{u_2}\ddot{u}_2 = 0, \tag{15f}$$

$$\delta v_2 : \frac{\partial \mathcal{P}_{xy}}{\partial x} + \frac{\partial \mathcal{P}_{yy}}{\partial y} - \mathcal{P}_{yz} - \mathcal{I}_0^{v_2}\ddot{v}_0 - \mathcal{I}_1^{v_2}\ddot{v}_1 - \mathcal{I}_2^{v_2}\ddot{v}_2 = 0. \tag{15g}$$

Furthermore, the natural boundary conditions associated with the variations in displacement components are given by the following equations:

$$\delta u_0 = 0 \quad \text{or} \quad \mathcal{N}_{xx}\hat{n}_x + \mathcal{N}_{xy}\hat{n}_y = 0, \tag{16a}$$

$$\delta v_0 = 0 \quad \text{or} \quad \mathcal{N}_{xy}\hat{n}_x + \mathcal{N}_{yy}\hat{n}_y = 0, \tag{16b}$$

$$\delta w_0 = 0 \quad \text{or} \quad \left(\mathcal{N}_{xz} + \mathcal{N}_{xx}\frac{\partial w_0}{\partial x} + \mathcal{N}_{xy}\frac{\partial w_0}{\partial y}\right)\hat{n}_x + \left(\mathcal{N}_{yz} + \mathcal{N}_{yy}\frac{\partial w_0}{\partial y} + \mathcal{N}_{xy}\frac{\partial w_0}{\partial x}\right)\hat{n}_y = 0, \tag{16c}$$

$$\delta u_1 = 0 \quad \text{or} \quad \mathcal{M}_{xx}\hat{n}_x + \mathcal{M}_{xy}\hat{n}_y = 0, \tag{16d}$$

$$\delta v_1 = 0 \quad \text{or} \quad \mathcal{M}_{xy}\hat{n}_x + \mathcal{M}_{yy}\hat{n}_y = 0, \tag{16e}$$

$$\delta u_2 = 0 \quad \text{or} \quad \mathcal{P}_{xx}\hat{n}_x + \mathcal{P}_{xy}\hat{n}_y = 0, \tag{16f}$$

$$\delta v_2 = 0 \quad \text{or} \quad \mathcal{P}_{xy}\hat{n}_x + \mathcal{P}_{yy}\hat{n}_y = 0, \tag{16g}$$

where

$$\begin{bmatrix} \mathcal{N}_{xx} \\ \mathcal{N}_{yy} \\ \mathcal{N}_{xy} \end{bmatrix} = \int\int \begin{bmatrix} \sigma_{xx} \\ \sigma_{yy} \\ \tau_{xy} \end{bmatrix} dV, \quad \begin{bmatrix} \mathcal{M}_{xx} \\ \mathcal{M}_{yy} \\ \mathcal{M}_{xy} \end{bmatrix} = \int \mathcal{F}(z) \times \begin{bmatrix} \sigma_{xx} \\ \sigma_{yy} \\ \delta u_{xy} \end{bmatrix} dV,$$

$$\begin{bmatrix} \mathcal{P}_{xx} \\ \mathcal{P}_{yy} \\ \mathcal{P}_{xy} \end{bmatrix} = \int \mathcal{G}(z) \times \begin{bmatrix} \sigma_{xx} \\ \sigma_{yy} \\ \tau_{xy} \end{bmatrix} dV, \quad \begin{bmatrix} \mathcal{N}_{xz} \\ \mathcal{N}_{yz} \end{bmatrix} = \int \begin{bmatrix} \delta u_{xz} \\ \delta u_{yz} \end{bmatrix} dV,$$

$$\begin{bmatrix} \mathcal{M}_{xz} \\ \mathcal{M}_{yz} \end{bmatrix} = \int \mathcal{F}'(z) \times \begin{bmatrix} \delta u_{xz} \\ \delta u_{yz} \end{bmatrix} dV, \quad \begin{bmatrix} \mathcal{P}_{xz} \\ \mathcal{P}_{yz} \end{bmatrix} = \int \mathcal{G}'(z) \times \begin{bmatrix} \delta u_{xz} \\ \delta u_{yz} \end{bmatrix} dV,$$

$$\{\mathcal{I}_0^{u_0}, \mathcal{I}_1^{u_0}, \mathcal{I}_2^{u_0}\} = \int_V (\{1, z, \mathcal{F}(z)\}\rho(x, y, z))dxdydz,$$

$$\{\mathcal{I}_0^{u_1}, \mathcal{I}_1^{u_1}, \mathcal{I}_2^{u_1}\} = \int_V (\mathcal{F}(z) \times \{1, \mathcal{F}(z), \mathcal{G}(z)\}\rho(x, y, z))dxdydz,$$

$$\{\mathcal{I}_0^{u_2}, \mathcal{I}_1^{u_2}, \mathcal{I}_2^{u_2}\} = \int_V (\mathcal{G}(z) \times \{1, \mathcal{F}(z), \mathcal{G}(z)\}\,\rho(x, y, z))dxdydz,$$

$$\{\mathcal{I}_0^{v_0}, \mathcal{I}_1^{v_0}, \mathcal{I}_2^{v_0}\} = \int_V (\{1, z, \mathcal{F}(z)\}\rho(x, y, z))dxdydz,$$

$$\{\mathcal{I}_0^{v_1}, \mathcal{I}_1^{v_1}, \mathcal{I}_2^{v_1}\} = \int_V (\mathcal{F}(z) \times \{1, \mathcal{F}(z), \mathcal{G}(z)\}\rho(x, y, z))dxdydz,$$

$$\{\mathcal{I}_0^{v_2}, \mathcal{I}_1^{v_2}, \mathcal{I}_2^{v_2}\} = \int_V (G(z) \times \{1, \mathcal{F}(z), \mathcal{G}(z)\}\rho(x, y, z))dxdydz,$$

$$\mathcal{I}_0^{w_0} = \int_V (\rho(x, y, z))dxdydz. \tag{17}$$

The equations expressed explicitly through the displacement components take the following final form:

$$\delta u_0 : (1 - l^2\nabla^2)\left(\frac{\partial \mathcal{N}_{xx}}{\partial x} + \frac{\partial \mathcal{N}_{xy}}{\partial y}\right) + (1 - \mu^2\nabla^2)(-\mathcal{I}_0^{u_0}\ddot{u}_0 - \mathcal{I}_1^{u_0}\ddot{u}_1 - \mathcal{I}_2^{u_0}\ddot{u}_2) = 0, \tag{18a}$$

$$\delta v_0 : (1-l^2\nabla^2)\left(\frac{\partial \mathcal{N}_{xy}}{\partial x}+\frac{\partial \mathcal{N}_{yy}}{\partial y}\right)+(1-\mu^2\nabla^2)(-\mathcal{J}_0^{v_0}\ddot{v}_0-\mathcal{J}_1^{v_0}\ddot{v}_1-\mathcal{J}_2^{v_0}\ddot{v}_2)=0, \tag{18b}$$

$$\delta w_0 : (1-l^2\nabla^2)\left(\begin{array}{l}\dfrac{\partial \mathcal{N}_{xx}}{\partial x}+\dfrac{\partial \mathcal{N}_{yx}}{\partial y}+\dfrac{\partial}{\partial x}\left(\mathcal{N}_{xx}\dfrac{\partial w_0}{\partial x}\right)+\dfrac{\partial}{\partial y}\left(\mathcal{N}_{yy}\dfrac{\partial w_0}{\partial y}\right)\\ \quad+\dfrac{\partial}{\partial x}\left(\mathcal{N}_{xy}\dfrac{\partial w_0}{\partial y}\right)+\dfrac{\partial}{\partial y}\left(\mathcal{N}_{xy}\dfrac{\partial w_0}{\partial x}\right)\end{array}\right)$$
$$+(1-\mu^2\nabla^2)(-\mathcal{J}_0^{w_0}\ddot{w}_0)=0, \tag{18c}$$

$$\delta u_1 : (1-l^2\nabla^2)\left(\frac{\partial \mathcal{M}_{xx}}{\partial x}+\frac{\partial \mathcal{M}_{xy}}{\partial y}-\mathcal{M}_{xz}\right)$$
$$+(1-\mu^2\nabla^2)\begin{pmatrix}-\mathcal{J}_0^{u_1}\ddot{u}_0-\mathcal{J}_1^{u_1}\ddot{u}_1\\ -\mathcal{J}_2^{u_1}\ddot{u}_2\end{pmatrix}=0, \tag{18d}$$

$$\delta v_1 : (1-l^2\nabla^2)\left(\frac{\partial \mathcal{M}_{xy}}{\partial x}+\frac{\partial \mathcal{M}_{yy}}{\partial y}-\mathcal{M}_{yz}\right)$$
$$+(1-\mu^2\nabla^2)(-\mathcal{J}_0^{v_1}\ddot{v}_0-\mathcal{J}_1^{v_1}\ddot{v}_1-\mathcal{J}_2^{v_1}\ddot{v}_2)=0, \tag{18e}$$

$$\delta u_2 : (1-l^2\nabla^2)\left(\frac{\partial \mathcal{P}_{xx}}{\partial x}+\frac{\partial \mathcal{P}_{xy}}{\partial y}-\mathcal{P}_{xz}\right)$$
$$+(1-\mu^2\nabla^2)(-\mathcal{J}_0^{u_2}\ddot{u}_0-\mathcal{J}_1^{u_2}\ddot{u}_1-\mathcal{J}_2^{u_2}\ddot{u}_2)=0, \tag{18f}$$

$$\delta v_2 : (1-l^2\nabla^2)\left(\frac{\partial \mathcal{P}_{xy}}{\partial x}+\frac{\partial \mathcal{P}_{yy}}{\partial y}-\mathcal{P}_{yz}\right)$$
$$+(1-\mu^2\nabla^2)(-\mathcal{J}_0^{v_2}\ddot{v}_0-\mathcal{J}_1^{v_2}\ddot{v}_1-\mathcal{J}_2^{v_2}\ddot{v}_2)=0. \tag{18g}$$

2.6. *Theoretical formulation and coordinate mapping*

The coordinate system of this transformed domain is represented by (ξ,η). This mapping process aligns with the standard practice of converting an isoparametric element into a standard element within the finite element method. The transformation is carried out using the following relation.[26]

This approach uses the coordinates of the four corner nodes (x_i, y_i) for $i = 1,2,3,4$ in the physical domain, along with the shape functions $\mathcal{H}_i(\xi,\eta)$ associated with each node, which are defined as follows[26]:

$$\mathcal{H}_i=(-1)^{i+1}(1-\xi_i-\xi)(1-\eta_i-\eta), \quad i=1,2,3,4. \tag{19}$$

Using the chain rule, the first- and second-order derivatives of any function with respect to x, y can be converted into derivatives with respect to ξ, η. Consequently, the transformation matrices are formulated as follows[26]:

$$\begin{Bmatrix} \dfrac{\partial\{\}}{\partial x} \\ \dfrac{\partial\{\}}{\partial y} \end{Bmatrix} = \mathcal{J}_{11}^{-1} \begin{Bmatrix} \dfrac{\partial\{\}}{\partial \xi} \\ \dfrac{\partial\{\}}{\partial \eta} \end{Bmatrix} \begin{Bmatrix} \dfrac{\partial^2\{\}}{\partial x^2} \\ \dfrac{\partial^2\{\}}{\partial y^2} \\ \dfrac{\partial^2\{\}}{\partial x \partial y} \end{Bmatrix} = -\mathcal{J}_{22}^{-1}\mathcal{J}_{21}\mathcal{J}_{11}^{-1} \begin{Bmatrix} \dfrac{\partial\{\}}{\partial \xi} \\ \dfrac{\partial\{\}}{\partial \eta} \end{Bmatrix} + \mathcal{J}_{22}^{-1} \begin{Bmatrix} \dfrac{\partial^2\{\}}{\partial \xi^2} \\ \dfrac{\partial^2\{\}}{\partial \eta^2} \\ \dfrac{\partial^2\{\}}{\partial \xi \partial \eta} \end{Bmatrix}, \tag{20}$$

in which,

$$\mathcal{J}_{11} = \begin{bmatrix} \dfrac{\partial x}{\partial \xi} & \dfrac{\partial y}{\partial \xi} \\ \dfrac{\partial x}{\partial \eta} & \dfrac{\partial y}{\partial \eta} \end{bmatrix}, \quad \mathcal{J}_{21} = \begin{bmatrix} \dfrac{\partial^2 x}{\partial \xi^2} & \dfrac{\partial^2 y}{\partial \xi^2} \\ \dfrac{\partial^2 x}{\partial \eta^2} & \dfrac{\partial^2 y}{\partial \eta^2} \\ \dfrac{\partial^2 x}{\partial \xi \partial \eta} & \dfrac{\partial^2 y}{\partial \xi \partial \eta} \end{bmatrix},$$

$$\mathcal{J}_{22} = \begin{bmatrix} \left(\dfrac{\partial x}{\partial \xi}\right)^2 & \left(\dfrac{\partial y}{\partial \xi}\right)^2 & \dfrac{\partial x}{\partial \xi}\dfrac{\partial y}{\partial \xi} \\ \left(\dfrac{\partial x}{\partial \eta}\right)^2 & \left(\dfrac{\partial y}{\partial \eta}\right)^2 & \dfrac{\partial x}{\partial \eta}\dfrac{\partial y}{\partial \eta} \\ \dfrac{\partial x}{\partial \xi}\dfrac{\partial x}{\partial \eta} & \dfrac{\partial y}{\partial \xi}\dfrac{\partial y}{\partial \eta} & \dfrac{1}{2}\left(\dfrac{\partial x}{\partial \xi}\dfrac{\partial y}{\partial \eta} + \dfrac{\partial x}{\partial \eta}\dfrac{\partial y}{\partial \xi}\right) \end{bmatrix}. \tag{21}$$

Using the transformation matrices described above, the equations of motion can be reformulated within the $\xi - \eta$ coordinate system. Moreover, while the differential area element is represented as $dxdy$ in the $x - y$ coordinate system, its counterpart in the transformed computational domain is expressed as follows[26]:

$$dxdy = |\mathcal{J}_{11}| d\xi d\eta. \tag{22}$$

Here, $|\mathcal{J}_{11}|$ represents the determinant of the matrix $\mathcal{J}_{11}$.

3. Solution Procedure

Considering the problem's geometry and boundary conditions, an effective approach for the solution is to express the displacement using a harmonic representation, given

by the following equation[27]:

$$\begin{aligned}
&u_0 = \mathcal{U}_0 \exp(kx + ky)i, \quad v_0 = \mathcal{V}_0 \exp(kx + ky)i, \quad w_0 = \mathcal{W}_0 \exp(kx + ky)i,\\
&u_1 = \mathcal{U}_1 \exp(kx + ky)i, \quad v_1 = \mathcal{V}_1 \exp(kx + ky)i, \quad u_2 = \mathcal{U}_2 \exp(kx + ky)i,\\
&v_2 = \mathcal{V}_2 \exp(kx + ky)i.
\end{aligned} \tag{23}$$

Substituting Eqs. (17), (20), (21), (22), and (23) into Eqs. (18a)–(18g) leads to the derivation of a system of ordinary differential equations.

$$\begin{aligned}
&\mathcal{K}_{11}\mathcal{U}_0(t) + \mathcal{K}_{12}\mathcal{V}_0(t) + \mathcal{K}_{13}\mathcal{W}_0(t) + \mathcal{K}_{14}\mathcal{W}_0^2(t) + \mathcal{K}_{15}\mathcal{U}_1(t) + \mathcal{K}_{16}\mathcal{V}_1(t)\\
&\quad + \mathcal{K}_{17}\mathcal{U}_2(t) + \mathcal{K}_{18}\mathcal{V}_2(t) = m_{11}\ddot{\mathcal{U}}_0(t) + m_{12}\ddot{\mathcal{V}}_0(t) + m_{13}\ddot{\mathcal{W}}_0(t) + m_{14}\ddot{\mathcal{U}}_1(t)\\
&\quad + m_{15}\ddot{\mathcal{V}}_1(t) + m_{16}\ddot{\mathcal{U}}_2(t) + m_{17}\ddot{\mathcal{V}}_2(t),
\end{aligned} \tag{24a}$$

$$\begin{aligned}
&\mathcal{K}_{21}\mathcal{U}_0(t) + \mathcal{K}_{22}\mathcal{V}_0(t) + \mathcal{K}_{23}\mathcal{W}_0(t) + \mathcal{K}_{24}\mathcal{W}_0^2(t) + \mathcal{K}_{25}\mathcal{U}_1(t) + \mathcal{K}_{26}\mathcal{V}_1(t)\\
&\quad + \mathcal{K}_{27}\mathcal{U}_2(t) + \mathcal{K}_{28}\mathcal{V}_2(t) = m_{21}\ddot{\mathcal{U}}_0(t) + m_{22}\ddot{\mathcal{V}}_0(t) + m_{23}\ddot{\mathcal{W}}_0(t) + m_{24}\ddot{\mathcal{U}}_1(t)\\
&\quad + m_{25}\ddot{\mathcal{V}}_1(t) + m_{26}\ddot{\mathcal{U}}_2(t) + m_{27}\ddot{\mathcal{V}}_2(t),
\end{aligned} \tag{24b}$$

$$\begin{aligned}
&\mathcal{K}_{31}\mathcal{U}_0(t) + \mathcal{K}_{32}\mathcal{V}_0(t) + \mathcal{K}_{33}\mathcal{W}_0(t) + \mathcal{K}_{34}\mathcal{W}_0^2(t) + \mathcal{K}_{35}\mathcal{W}_0^3(t) + \mathcal{K}_{36}\mathcal{U}_1(t)\\
&\quad + \mathcal{K}_{37}\mathcal{V}_1(t) + \mathcal{K}_{38}\mathcal{U}_2(t) + \mathcal{K}_{39}\mathcal{V}_2(t) + \mathcal{K}_{310}\mathcal{U}_0(t)\mathcal{W}_0(t) + \mathcal{K}_{311}\mathcal{V}_0(t)\mathcal{W}_0(t)\\
&\quad + \mathcal{K}_{312}\mathcal{U}_1(t)\mathcal{W}_0(t) + \mathcal{K}_{313}\mathcal{V}_1(t)\mathcal{W}_0(t) + \mathcal{K}_{314}\mathcal{U}_2(t)\mathcal{W}_0(t) + \mathcal{K}_{315}\mathcal{V}_2(t)\mathcal{W}_0(t)\\
&= m_{31}\ddot{\mathcal{U}}_0(t) + m_{32}\ddot{\mathcal{V}}_0(t) + m_{33}\ddot{\mathcal{W}}_0(t) + m_{34}\ddot{\mathcal{U}}_1(t) + m_{35}\ddot{\mathcal{V}}_1(t) + m_{36}\ddot{\mathcal{U}}_2(t)\\
&\quad + m_{37}\ddot{\mathcal{V}}_2(t),
\end{aligned} \tag{24c}$$

$$\begin{aligned}
&\mathcal{K}_{41}\mathcal{U}_0(t) + \mathcal{K}_{42}\mathcal{V}_0(t) + \mathcal{K}_{43}\mathcal{W}_0(t) + \mathcal{K}_{44}\mathcal{W}_0^2(t) + \mathcal{K}_{45}\mathcal{U}_1(t) + \mathcal{K}_{46}\mathcal{V}_1(t)\\
&\quad + \mathcal{K}_{47}\mathcal{U}_2(t) + \mathcal{K}_{48}\mathcal{V}_2(t) = m_{41}\ddot{\mathcal{U}}_0(t) + m_{42}\ddot{\mathcal{V}}_0(t) + m_{43}\ddot{\mathcal{W}}_0(t) + m_{44}\ddot{\mathcal{U}}_1(t)\\
&\quad + m_{45}\ddot{\mathcal{V}}_1(t) + m_{46}\ddot{\mathcal{U}}_2(t) + m_{47}\ddot{\mathcal{V}}_2(t),
\end{aligned} \tag{24d}$$

$$\begin{aligned}
&\mathcal{K}_{51}\mathcal{U}_0(t) + \mathcal{K}_{52}\mathcal{V}_0(t) + \mathcal{K}_{53}\mathcal{W}_0(t) + \mathcal{K}_{54}\mathcal{W}_0^2(t) + \mathcal{K}_{55}\mathcal{U}_1(t) + \mathcal{K}_{56}\mathcal{V}_1(t)\\
&\quad + \mathcal{K}_{57}\mathcal{U}_2(t) + \mathcal{K}_{58}\mathcal{V}_2(t) = m_{51}\ddot{\mathcal{U}}_0(t) + m_{52}\ddot{\mathcal{V}}_0(t) + m_{53}\ddot{\mathcal{W}}_0(t) + m_{54}\ddot{\mathcal{U}}_1(t)\\
&\quad + m_{55}\ddot{\mathcal{V}}_1(t) + m_{56}\ddot{\mathcal{U}}_2(t) + m_{57}\ddot{\mathcal{V}}_2(t),
\end{aligned} \tag{24e}$$

$$\begin{aligned}
&\mathcal{K}_{61}\mathcal{U}_0(t) + \mathcal{K}_{62}\mathcal{V}_0(t) + \mathcal{K}_{63}\mathcal{W}_0(t) + \mathcal{K}_{64}\mathcal{W}_0^2(t) + \mathcal{K}_{65}\mathcal{U}_1(t) + \mathcal{K}_{66}\mathcal{V}_1(t)\\
&\quad + \mathcal{K}_{67}\mathcal{U}_2(t) + \mathcal{K}_{68}\mathcal{V}_2(t) = m_{61}\ddot{\mathcal{U}}_0(t) + m_{62}\ddot{\mathcal{V}}_0(t) + m_{63}\ddot{\mathcal{W}}_0(t) + m_{64}\ddot{\mathcal{U}}_1(t)\\
&\quad + m_{65}\ddot{\mathcal{V}}_1(t) + m_{66}\ddot{\mathcal{U}}_2(t) + m_{67}\ddot{\mathcal{V}}_2(t),
\end{aligned} \tag{24f}$$

$$\mathcal{K}_{81}\mathcal{U}_0(t) + \mathcal{K}_{82}\mathcal{V}_0(t) + \mathcal{K}_{83}\mathcal{W}_0(t) + \mathcal{K}_{84}\mathcal{W}_0^2(t) + \mathcal{K}_{85}\mathcal{U}_1(t) + \mathcal{K}_{86}\mathcal{V}_1(t) + \mathcal{K}_{87}\mathcal{U}_2(t) + \mathcal{K}_{88}\mathcal{V}_2(t) = m_{81}\ddot{\mathcal{U}}_0(t) + m_{82}\ddot{\mathcal{V}}_0(t) + m_{83}\ddot{\mathcal{W}}_0(t) + m_{84}\ddot{\mathcal{U}}_1(t) + m_{85}\ddot{\mathcal{V}}_1(t) + m_{86}\ddot{\mathcal{U}}_2(t) + m_{87}\ddot{\mathcal{V}}_2(t). \tag{24g}$$

Since the inertia terms $\ddot{\mathcal{U}}_0(t)$, $\ddot{\mathcal{V}}_0(t)$, $\ddot{\mathcal{W}}_0(t)$, $\ddot{\mathcal{U}}_1(t)$, $\ddot{\mathcal{V}}_1(t)$, $\ddot{\mathcal{U}}_2(t)$, and $\ddot{\mathcal{V}}_2$ have negligible influence, they are omitted from Eqs. (24a), (24b), (24d), (24e), (24f), and (24g). These equations can then be solved independently, and the resulting solutions are substituted back into Eq. (24c).

$$\ddot{\mathcal{W}}_0(t) + \tilde{\jmath}_1\mathcal{W}_0(t) + \tilde{\jmath}_2\mathcal{W}_0^2(t) + \tilde{\jmath}_3\mathcal{W}_0^3(t) = 0. \tag{25}$$

Here, $\tilde{\jmath}_1$ through $\tilde{\jmath}_3$ represent both linear and nonlinear components related to $\mathcal{W}_0$. Using the harmonic balance method, $\mathcal{W}_0$ can be approximated by the following expression:

$$\mathcal{W}_0(t) = \sum_{k=0}^{\mathcal{M}} \mathfrak{A}_k \cos(\mathfrak{k}\eta). \tag{26}$$

In this expression, $\mathfrak{A}_1$ is a constant, while $\mathfrak{A}_i (i = 0, 2, 3, \ldots, \mathcal{M})$ are unknown functions that vary with time. The variable η is defined as $\omega t + \theta$, where θr represents the initial phase angle, and ω denotes the nonlinear natural frequency of the nanoplates. Since the amplitude of the nanoplates depends on this nonlinear frequency, ω itself is time-dependent during damped vibrations, expressed as $\omega = \omega(t)$. For the following analysis, the parameter $\mathcal{M}$ in Eq. (26) is set to six, so the equation can be rewritten accordingly.

$$\tilde{\mathcal{W}}(t) = (\mathfrak{A}_0 + \mathfrak{A}_1\cos\eta + \mathfrak{A}_2\cos 2\eta + \mathfrak{A}_3\cos 3\eta + \mathfrak{A}_4\cos 4\eta + \mathfrak{A}_5\cos 5\eta + \mathfrak{A}_6\cos 6\eta). \tag{27}$$

By substituting Eq. (27) into Eq. (25) and equating the coefficients of $\cos(k\eta)$ to zero, the following equation is derived.

$$\cos(\mathfrak{k}\eta) : \left\{\gamma_{11} - \mathfrak{k}^2\left(\omega + t\frac{d\omega}{dt}\right)^2\right\}\mathfrak{A}_{\mathfrak{k}} + \gamma_{12}\mathcal{R}_{\mathfrak{k}1} + \gamma_{13}\mathcal{R}_{\mathfrak{k}2} = 0, \quad (\mathfrak{k} = 0, 1, 2, 3, 4, 5, 6). \tag{28}$$

Here, $\gamma_{11} = \jmath_1$, $\gamma_{12} = \tilde{\jmath}_2$ and $\gamma_{13} = \tilde{\jmath}_3$; the functions $\mathcal{R}_{\mathfrak{k}1}$ and $\mathcal{R}_{\mathfrak{k}2}$ are associated with the parameter $\mathcal{U}_k$, with their detailed forms given in Eqs. (29a)–(29u).

$$\mathcal{R}_{01} = \mathfrak{A}_0^2 + \frac{1}{2}\mathfrak{A}_1^2 + \frac{1}{2}\mathfrak{A}_2^2 + \frac{1}{2}\mathfrak{A}_3^2 + \frac{1}{2}\mathfrak{A}_4^2 + \frac{1}{2}\mathfrak{A}_5^2 + \frac{1}{2}\mathfrak{A}_6^2, \tag{29a}$$

$$\mathcal{R}_{11} = 2\mathfrak{A}_0\mathfrak{A}_1 + \mathfrak{A}_1\mathfrak{A}_2 + \mathfrak{A}_2\mathfrak{A}_3 + \mathfrak{A}_3\mathfrak{A}_4 + \mathfrak{A}_4\mathfrak{A}_5 + \mathfrak{A}_5\mathfrak{A}_6, \tag{29b}$$

$$\mathcal{R}_{21} = \frac{1}{2}\mathfrak{A}_1^2 + \mathfrak{A}_1\mathfrak{A}_3 + 2\mathfrak{A}_0\mathfrak{A}_2 + \mathfrak{A}_2\mathfrak{A}_4 + \mathfrak{A}_3\mathfrak{A}_5 + \mathfrak{A}_4\mathfrak{A}_6, \tag{29c}$$

$$\mathcal{R}_{31} = 2\mathfrak{A}_0\mathfrak{A}_3 + \mathfrak{A}_1\mathfrak{A}_2 + \mathfrak{A}_1\mathfrak{A}_4 + \mathfrak{A}_2\mathfrak{A}_5 + \mathfrak{A}_3\mathfrak{A}_6, \tag{29d}$$

$$\mathcal{R}_{41} = \frac{1}{2}\mathfrak{A}_2^2 + \mathfrak{A}_2\mathfrak{A}_6 + 2\mathfrak{A}_0\mathfrak{A}_4 + \mathfrak{A}_1\mathfrak{A}_3 + \mathfrak{A}_1\mathfrak{A}_5, \tag{29e}$$

$$\mathcal{R}_{51} = 2\mathfrak{A}_0\mathfrak{A}_5 + \mathfrak{A}_1\mathfrak{A}_4 + \mathfrak{A}_2\mathfrak{A}_3 + \mathfrak{A}_1\mathfrak{A}_6, \tag{29f}$$

$$\mathcal{R}_{61} = \frac{1}{2}\mathfrak{A}_3^2 + 2\mathfrak{A}_0\mathfrak{A}_6 + \mathfrak{A}_1\mathfrak{A}_5 + \mathfrak{A}_2\mathfrak{A}_4, \tag{29g}$$

$$\begin{aligned}\mathcal{R}_{02} = {} & \mathfrak{A}_0^3 + \frac{3}{4}\mathfrak{A}_1^2\mathfrak{A}_2 + \frac{3}{4}\mathfrak{A}_2^2\mathfrak{A}_4 + \frac{3}{4}\mathfrak{A}_3^2\mathfrak{A}_6 + \frac{3}{2}\mathfrak{A}_0\mathfrak{A}_1^2 + \frac{3}{2}\mathfrak{A}_0\mathfrak{A}_2^2 + \frac{3}{2}\mathfrak{A}_0\mathfrak{A}_3^2 \\ & + \frac{3}{2}\mathfrak{A}_0\mathfrak{A}_4^2 + \frac{3}{2}\mathfrak{A}_0\mathfrak{A}_5^2 + \frac{3}{2}\mathfrak{A}_0\mathfrak{A}_6^2 + \frac{3}{2}\mathfrak{A}_1\mathfrak{A}_2\mathfrak{A}_3 + \frac{3}{2}\mathfrak{A}_1\mathfrak{A}_3\mathfrak{A}_4 + \frac{3}{2}\mathfrak{A}_1\mathfrak{A}_4\mathfrak{A}_5 \\ & + \frac{3}{2}\mathfrak{A}_1\mathfrak{A}_5\mathfrak{A}_6 + \frac{3}{2}\mathfrak{A}_2\mathfrak{A}_3\mathfrak{A}_5 + \frac{3}{2}\mathfrak{A}_2\mathfrak{A}_4\mathfrak{A}_6,\end{aligned} \tag{29h}$$

$$\begin{aligned}\mathcal{R}_{12} = {} & \frac{3}{4}\mathfrak{A}_1^3 + 3\mathfrak{A}_0^2\mathfrak{A}_1 + \frac{3}{4}\mathfrak{A}_1^2\mathfrak{A}_3 + \frac{3}{4}\mathfrak{A}_2^2\mathfrak{A}_3 + \frac{3}{4}\mathfrak{A}_2^2\mathfrak{A}_5 + \frac{3}{4}\mathfrak{A}_3^2\mathfrak{A}_5 + \frac{3}{2}\mathfrak{A}_1\mathfrak{A}_2^2 \\ & + \frac{3}{2}\mathfrak{A}_1\mathfrak{A}_3^2 + \frac{3}{2}\mathfrak{A}_1\mathfrak{A}_4^2 + \frac{3}{2}\mathfrak{A}_1\mathfrak{A}_5^2 + \frac{3}{2}\mathfrak{A}_1\mathfrak{A}_6^2 + 3\mathfrak{A}_0\mathfrak{A}_1\mathfrak{A}_2 + 3\mathfrak{A}_0\mathfrak{A}_2\mathfrak{A}_3 \\ & + 3\mathfrak{A}_0\mathfrak{A}_3\mathfrak{A}_4 + 3\mathfrak{A}_0\mathfrak{A}_4\mathfrak{A}_5 + 3\mathfrak{A}_0\mathfrak{A}_5\mathfrak{A}_6 + \frac{3}{2}\mathfrak{A}_1\mathfrak{A}_2\mathfrak{A}_4 + \frac{3}{2}\mathfrak{A}_1\mathfrak{A}_3\mathfrak{A}_5 \\ & + \frac{3}{2}\mathfrak{A}_1\mathfrak{A}_4\mathfrak{A}_6 + \frac{3}{2}\mathfrak{A}_2\mathfrak{A}_3\mathfrak{A}_4 + \frac{3}{2}\mathfrak{A}_2\mathfrak{A}_3\mathfrak{A}_6 + \frac{3}{2}\mathfrak{A}_2\mathfrak{A}_4\mathfrak{A}_5 + \frac{3}{2}\mathfrak{A}_2\mathfrak{A}_5\mathfrak{A}_6 \\ & + \frac{3}{2}\mathfrak{A}_3\mathfrak{A}_4\mathfrak{A}_6,\end{aligned} \tag{29i}$$

$$\begin{aligned}\mathcal{R}_{22} = {} & \frac{3}{4}\mathfrak{A}_2^3 + 3\mathfrak{A}_0^2\mathfrak{A}_2 + \frac{3}{2}\mathfrak{A}_1^2\mathfrak{A}_2 + \frac{3}{4}\mathfrak{A}_1^2\mathfrak{A}_4 + \frac{3}{4}\mathfrak{A}_2^2\mathfrak{A}_6 + \frac{3}{4}\mathfrak{A}_3^2\mathfrak{A}_4 + \frac{3}{4}\mathfrak{A}_4^2\mathfrak{A}_6 \\ & + \frac{3}{2}\mathfrak{A}_0\mathfrak{A}_1^2 + \frac{3}{2}\mathfrak{A}_2\mathfrak{A}_3^2 + \frac{3}{2}\mathfrak{A}_2\mathfrak{A}_4^2 + \frac{3}{2}\mathfrak{A}_2\mathfrak{A}_5^2 + \frac{3}{2}\mathfrak{A}_2\mathfrak{A}_6^2 + 3\mathfrak{A}_0\mathfrak{A}_1\mathfrak{A}_3 \\ & + 3\mathfrak{A}_0\mathfrak{A}_2\mathfrak{A}_4 + 3\mathfrak{A}_0\mathfrak{A}_3\mathfrak{A}_5 + 3\mathfrak{A}_0\mathfrak{A}_4\mathfrak{A}_6 + \frac{3}{2}\mathfrak{A}_1\mathfrak{A}_2\mathfrak{A}_3 + \frac{3}{2}\mathfrak{A}_1\mathfrak{A}_2\mathfrak{A}_5 \\ & + \frac{3}{2}\mathfrak{A}_1\mathfrak{A}_3\mathfrak{A}_4 + \frac{3}{2}\mathfrak{A}_1\mathfrak{A}_3\mathfrak{A}_6 + \frac{3}{2}\mathfrak{A}_1\mathfrak{A}_4\mathfrak{A}_5 + \frac{3}{2}\mathfrak{A}_1\mathfrak{A}_5\mathfrak{A}_6 + \frac{3}{2}\mathfrak{A}_3\mathfrak{A}_4\mathfrak{A}_5 \\ & + \frac{3}{2}\mathfrak{A}_3\mathfrak{A}_5\mathfrak{A}_6,\end{aligned} \tag{29j}$$

$$\begin{aligned}\mathcal{R}_{32} = {} & \frac{1}{4}\mathfrak{A}_1^3 + \frac{3}{4}\mathfrak{A}_3^3 + 3\mathfrak{A}_0^2\mathfrak{A}_3 + \frac{3}{2}\mathfrak{A}_1^2\mathfrak{A}_3 + \frac{3}{4}\mathfrak{A}_1^2\mathfrak{A}_5 + \frac{3}{2}\mathfrak{A}_2^2\mathfrak{A}_3 + \frac{3}{4}\mathfrak{A}_4^2\mathfrak{A}_5 \\ & + \frac{3}{4}\mathfrak{A}_1\mathfrak{A}_2^2 + \frac{3}{2}\mathfrak{A}_3\mathfrak{A}_4^2 + \frac{3}{2}\mathfrak{A}_3\mathfrak{A}_5^2 + \frac{3}{2}\mathfrak{A}_3\mathfrak{A}_6^2 + 3\mathfrak{A}_0\mathfrak{A}_1\mathfrak{A}_2 + 3\mathfrak{A}_0\mathfrak{A}_1\mathfrak{A}_4\end{aligned}$$

$$+3\mathfrak{A}_0\mathfrak{A}_2\mathfrak{A}_5+3\mathfrak{A}_0\mathfrak{A}_3\mathfrak{A}_6+\frac{3}{2}\mathfrak{A}_1\mathfrak{A}_2\mathfrak{A}_4+\frac{3}{2}\mathfrak{A}_1\mathfrak{A}_2\mathfrak{A}_6+\frac{3}{2}\mathfrak{A}_1\mathfrak{A}_3\mathfrak{A}_5$$

$$+\frac{3}{2}\mathfrak{A}_1\mathfrak{A}_4\mathfrak{A}_6+\frac{3}{2}\mathfrak{A}_2\mathfrak{A}_3\mathfrak{A}_4+\frac{3}{2}\mathfrak{A}_2\mathfrak{A}_4\mathfrak{A}_5+\frac{3}{2}\mathfrak{A}_2\mathfrak{A}_5\mathfrak{A}_6+\frac{3}{2}\mathfrak{A}_4\mathfrak{A}_5\mathfrak{A}_6, \tag{29k}$$

$$\mathcal{R}_{42}=\frac{3}{4}\mathfrak{A}_4^3+3\mathfrak{A}_0^2\mathfrak{A}_4+\frac{3}{4}\mathfrak{A}_1^2\mathfrak{A}_2+\frac{3}{2}\mathfrak{A}_1^2\mathfrak{A}_4+\frac{3}{4}\mathfrak{A}_1^2\mathfrak{A}_6+\frac{3}{2}\mathfrak{A}_2^2\mathfrak{A}_4+\frac{3}{2}\mathfrak{A}_3^2\mathfrak{A}_4$$

$$+\frac{3}{4}\mathfrak{A}_5^2\mathfrak{A}_6+\frac{3}{2}\mathfrak{A}_0\mathfrak{A}_2^2+\frac{3}{4}\mathfrak{A}_2\mathfrak{A}_3^2+\frac{3}{2}\mathfrak{A}_4\mathfrak{A}_5^2+\frac{3}{2}\mathfrak{A}_4\mathfrak{A}_6^2+3\mathfrak{A}_0\mathfrak{A}_1\mathfrak{A}_3$$

$$+\mathfrak{A}_0\mathfrak{A}_1\mathfrak{A}_5+3\mathfrak{A}_0\mathfrak{A}_2\mathfrak{A}_6+\frac{3}{2}\mathfrak{A}_1\mathfrak{A}_2\mathfrak{A}_3+\frac{3}{2}\mathfrak{A}_1\mathfrak{A}_2\mathfrak{A}_5+\frac{3}{2}\mathfrak{A}_1\mathfrak{A}_3\mathfrak{A}_6$$

$$+\frac{3}{2}\mathfrak{A}_2\mathfrak{A}_3\mathfrak{A}_5+\frac{3}{2}\mathfrak{A}_2\mathfrak{A}_4\mathfrak{A}_6+\frac{3}{2}\mathfrak{A}_3\mathfrak{A}_4\mathfrak{A}_5+\frac{3}{2}\mathfrak{A}_3\mathfrak{A}_5\mathfrak{A}_6, \tag{29l}$$

$$\mathcal{R}_{52}=\frac{3}{4}\mathfrak{A}_5^3+3\mathfrak{A}_0^2\mathfrak{A}_5+\frac{3}{4}\mathfrak{A}_1^2\mathfrak{A}_3+\frac{3}{2}\mathfrak{A}_1^2\mathfrak{A}_5+\frac{3}{2}\mathfrak{A}_2^2\mathfrak{A}_5+\frac{3}{2}\mathfrak{A}_3^2\mathfrak{A}_5+\frac{3}{2}\mathfrak{A}_4^2\mathfrak{A}_5$$

$$+\frac{3}{4}\mathfrak{A}_1\mathfrak{A}_2^2+\frac{3}{4}\mathfrak{A}_1\mathfrak{A}_3^2+\frac{3}{4}\mathfrak{A}_3\mathfrak{A}_4^2+\frac{3}{2}\mathfrak{A}_5\mathfrak{A}_6^2+3\mathfrak{A}_0\mathfrak{A}_1\mathfrak{A}_4+3\mathfrak{A}_0\mathfrak{A}_1\mathfrak{A}_6$$

$$+3\mathfrak{A}_0\mathfrak{A}_2\mathfrak{A}_3+\frac{3}{2}\mathfrak{A}_1\mathfrak{A}_2\mathfrak{A}_4+\frac{3}{2}\mathfrak{A}_1\mathfrak{A}_2\mathfrak{A}_6+\frac{3}{2}\mathfrak{A}_2\mathfrak{A}_3\mathfrak{A}_4+\frac{3}{2}\mathfrak{A}_2\mathfrak{A}_3\mathfrak{A}_6$$

$$+\frac{3}{2}\mathfrak{A}_3\mathfrak{A}_4\mathfrak{A}_6+\frac{3}{2}\mathfrak{A}_4\mathfrak{A}_5\mathfrak{A}_6, \tag{29m}$$

$$\mathcal{R}_{62}=\frac{1}{4}\mathfrak{A}_2^3+3\mathfrak{A}_0^2\mathfrak{A}_6+\frac{3}{2}\mathfrak{A}_1^2\mathfrak{A}_6+\frac{3}{4}\mathfrak{A}_1^2\mathfrak{A}_4+\frac{3}{2}\mathfrak{A}_2^2\mathfrak{A}_6+\frac{3}{2}\mathfrak{A}_3^2\mathfrak{A}_6+\frac{3}{2}\mathfrak{A}_4^2\mathfrak{A}_6$$

$$+\frac{3}{2}\mathfrak{A}_5^2\mathfrak{A}_6+\frac{3}{4}\mathfrak{A}_6^3+\frac{3}{2}\mathfrak{A}_0\mathfrak{A}_3^2+\frac{3}{4}\mathfrak{A}_2\mathfrak{A}_4^2+\frac{3}{4}\mathfrak{A}_4\mathfrak{A}_5^2+3\mathfrak{A}_0\mathfrak{A}_1\mathfrak{A}_5+3\mathfrak{A}_0\mathfrak{A}_2\mathfrak{A}_4$$

$$+\frac{3}{2}\mathfrak{A}_1\mathfrak{A}_2\mathfrak{A}_3+\frac{3}{2}\mathfrak{A}_1\mathfrak{A}_2\mathfrak{A}_5+\frac{3}{2}\mathfrak{A}_1\mathfrak{A}_3\mathfrak{A}_4+\frac{3}{2}\mathfrak{A}_2\mathfrak{A}_3\mathfrak{A}_5+\frac{3}{2}\mathfrak{A}_3\mathfrak{A}_4\mathfrak{A}_5, \tag{29n}$$

$$\tilde{\mathcal{R}}_{02}^{(\hbar)}=\mathcal{R}_{02}^{(\hbar)}-\frac{3}{2}\mathfrak{A}_0^{(\hbar)}\mathfrak{A}_1^2, \tag{29o}$$

$$\tilde{\mathcal{R}}_{12}^{(\hbar)}=\mathcal{R}_{12}^{(\hbar)}-\frac{3}{4}\mathfrak{A}_1^3, \tag{29p}$$

$$\tilde{\mathcal{R}}_{22}^{(\hbar)}=\mathcal{R}_{22}^{(\hbar)}-\frac{3}{2}\mathfrak{A}_1^2\mathfrak{A}_2^{(\hbar)}, \tag{29q}$$

$$\tilde{\mathcal{R}}_{32}^{(\hbar)}=\mathcal{R}_{32}^{(\hbar)}-\frac{3}{2}\mathfrak{A}_1^2\mathfrak{A}_3^{(\hbar)}, \tag{29r}$$

$$\tilde{\mathcal{R}}_{42}^{(\hbar)}=\mathcal{R}_{42}^{(\hbar)}-\frac{3}{2}\mathfrak{A}_1^2\mathfrak{A}_4^{(\hbar)}, \tag{29s}$$

$$\tilde{\mathcal{R}}_{52}^{(\mathscr{k})} = \mathcal{R}_{52}^{(\mathscr{k})} - \frac{3}{2}\mathfrak{A}_1^2\mathfrak{A}_5^{(\mathscr{k})}, \tag{29t}$$

$$\tilde{\mathcal{R}}_{62}^{(\mathscr{k})} = \mathcal{R}_{62}^{(\mathscr{k})} - \frac{3}{2}\mathfrak{A}_1^2\mathfrak{A}_6^{(\mathscr{k})}. \tag{29u}$$

It is important to highlight that the coupled nonlinear equations presented in Eq. (28) are of particular significance. Due to their complexity, obtaining exact analytical solutions is nearly impossible. Therefore, an efficient iterative approach is employed to solve them, as outlined below:

$$\mathfrak{A}_k^{(i+1)} = \frac{\delta_{\mathscr{k}}\{\gamma_{12}(\mathscr{k}^2\mathcal{R}_{11}^{(i)}\mathfrak{A}_k^{(i)} - \mathcal{R}_{\mathscr{k}1}^{(i)}\mathfrak{A}_1) + \gamma_{13}(\mathscr{k}^2\tilde{\mathcal{R}}_{12}^{(i)}\mathfrak{A}_k^{(i)} - \tilde{\mathcal{R}}_{\mathscr{k}2}^{(i)}\mathfrak{A}_1)\}}{(\mathscr{k}^2-1)\gamma_{11}\mathfrak{A}_1 + \frac{3k^2-6}{4}\gamma_{13}\mathfrak{A}_1^3}, \quad (\mathscr{k} = 0, 2, 3, 4, 5, 6). \tag{30}$$

In this context, $\mathcal{R}_{ln}^{(i)}$ (for $l = 0, 1, 2, 3, 4, 5, 6$; $n = 1, 2$; $i = 0, 1, 2, \ldots$) represents the value of the ith iteration for $\mathcal{R}_{ln}$, and the variable $\tilde{\mathcal{R}}_{l2}^{(i)}$ is defined in Eqs. (29a–29u). Furthermore, the parameter $\delta_{\mathscr{k}}$ in Eq. (30) is given by the following equation:

$$\delta_{\mathscr{k}} = \begin{cases} +1, & \text{if } \mathscr{k} < 1, \\ -1, & \text{if } \mathscr{k} > 1. \end{cases} \tag{31}$$

The nonlinear natural frequency of a temperature-dependent functionally graded viscoelastic nanoplate can be determined by substituting the expressions for $\mathfrak{A}_i (i = 0, 2, 3, 4, 5, 6)$ into Eq. (28), specifically for the case when $\mathscr{k} = 1$.

$$\omega(t) = \begin{cases} \frac{1}{t}\int_0^t \sqrt{\gamma_{11} + \frac{\gamma_{12}\mathcal{R}_{11}(t) + \gamma_{13}\mathcal{R}_{12}(t)}{\mathfrak{A}_1}}dt, & t > 0 \\ \sqrt{\gamma_{11} + \frac{\gamma_{12}\mathcal{R}_{11}(t=0) + \gamma_{13}\mathcal{R}_{12}(t=0)}{\mathfrak{A}_1}}, & t = 0 \end{cases}, \tag{32a}$$

$$\omega(t)/\omega_0 = \begin{cases} \frac{1}{t}\int_0^t \sqrt{1 + \frac{\gamma_{12}\mathcal{R}_{11}(t) + \gamma_{13}\mathcal{R}_{12}(t)}{\gamma_{11}\mathfrak{A}_1}}dt, & t > 0 \\ \sqrt{1 + \frac{\gamma_{12}\mathcal{R}_{11}(t=0) + \gamma_{13}\mathcal{R}_{12}(t=0)}{\gamma_{11}\mathfrak{A}_1}}, & t = 0 \end{cases}. \tag{32b}$$

The linear natural frequency of the nanostructure, denoted by ω_0, is defined as $\omega_0 = \sqrt{\gamma}_{11}$. By applying Eqs. (30), (32a), and (32b), the expression for $\mathcal{W}_0$ in Eq. (27) can be simplified to a form that depends only on two unknowns: $\mathfrak{A}_1$ and θ. To determine these coefficients, the following initial conditions can be applied:

$$W_0(t=0) = A^*/h, \tag{33a}$$

$$\left.\frac{dW_0}{dt}\right|_{t=0} = 0. \tag{33b}$$

Here, $\mathfrak{A}^*$ denotes the initial displacement. At this stage, all variables have been determined, including θ and the coefficients $\mathfrak{A}_i$ for $i = 0, 1, \ldots, 6$. With these results, the nonlinear natural frequency of the nanoplate can be readily evaluated using Eqs. (32a) and (32b). Moreover, the nonlinear phase, and group velocities can be calculated using the following equation[28]:

$$\begin{aligned} \text{Phase velocity} &= \frac{\omega(t)}{k}, \\ \text{Group velocity} &= \frac{d\omega(t)}{dk}. \end{aligned} \tag{34}$$

4. Results and Discussion

4.1. *Validation*

Table 2 presents a comparative analysis of circular frequencies (ω) for various wave numbers (k), computed using the present study against values from Refs. 29–31. The material and geometric parameters are consistent across all sources: Poisson's ratio ($\nu = 0.3$), Young's modulus ($E = 210\,\text{GPa}$), density ($\rho = 7\,480\,\text{kg/m}^3$), and plate thickness ($h = 0.01\text{m}$). The wave numbers analyzed range from 2 to 23. While this study validates the model against existing numerical results, we acknowledge the absence of experimental data for further validation. Due to the lack of experimental test data for wave propagation in FGMs at the nanoscale, this study relies on comparisons with published numerical studies. As shown, the present method yields frequencies that closely align with those from the referenced works, exhibiting minimal deviation. For instance, at $k = 11$, the present result is 3824.08, while Refs. 29–31 report 3869.44, 3880.28, and 3863.09, respectively. This close agreement highlights the accuracy and reliability of the proposed methodology. The slight differences observed can be attributed to numerical precision, solution methods, or boundary condition implementations. These findings substantiate that the model effectively captures the dynamic response of the system under study. However, the

Table 2. Comparison of the current findings for circular frequencies (ω) with those reported in Refs. 29–31 ($\nu = 0.3$, $E = 210\,[\text{G}\mathcal{P}\text{a}]$, $\rho = 7\,480[\text{K}\mathcal{G}/\text{m}^3]$, $h = 0.01[\text{m}]$).

Wave number (k)	2	5	8	11	14	17	20	23
Present	126.89	792.57	2026.68	3824.08	6177.12	9077.80	12514.68	16475.00
Ref. 29	128.46	802.28	2050.90	3869.44	6250.88	9186.18	12664.47	16673.20
Ref. 30	128.27	801.71	2052.38	3880.28	6285.41	9267.77	12827.37	16964.19
Ref. 31	128.26	800.97	2047.55	3863.09	6240.55	9170.85	12643.1	16644.5

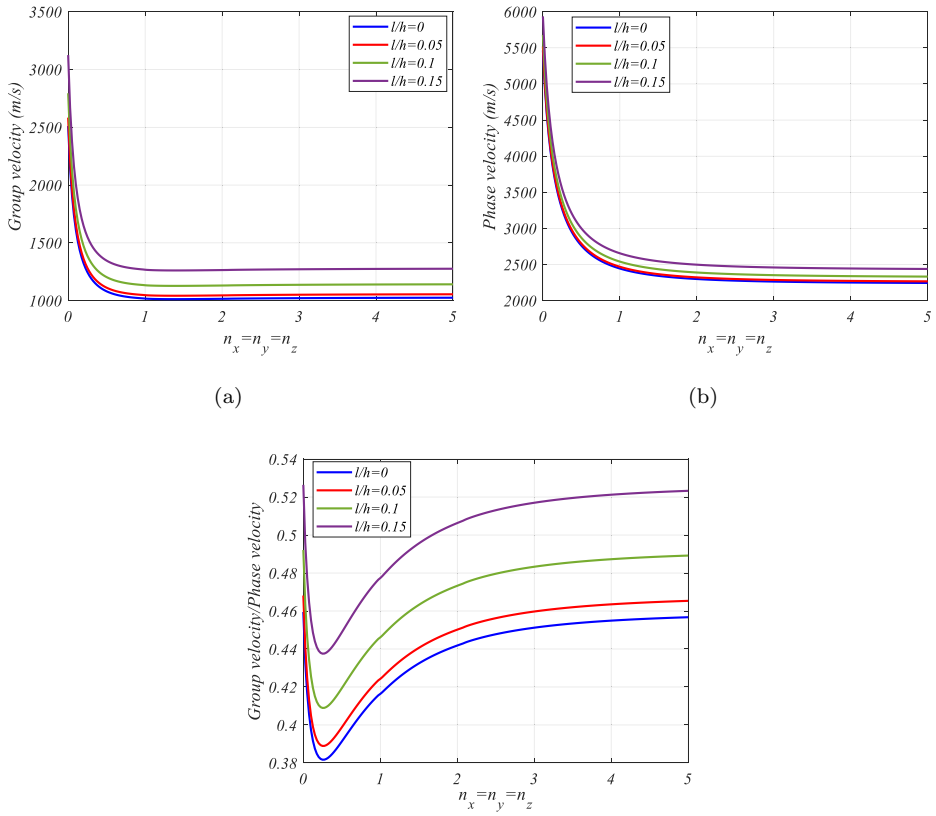

Fig. 2. The wave propagation characteristic as a function of the power index $n_x = n_y = n_z$ for different dimensionless length scale parameters.

absence of experimental validation remains a limitation, which will be addressed in future work through comparisons with available experimental data, if accessible.

4.2. *Parametric result*

Figure 2(a) presents the group velocity (1 000–3 500 m/s) as a function of the power index $n_x = n_y = n_z$ for different dimensionless length scale parameters ($\frac{l}{h} = 0, 0.05, 0.1, 0.15$). The results demonstrate that increasing the power index reduces phase velocity, indicating that stronger material gradation slows wave propagation. The inclusion of length scale effects ($l/h > 0$) further decreases phase velocity, highlighting the significance of small-scale interactions in nanostructures. The HHSDT effectively captures these trends, confirming its superiority over classical elasticity models. The reduction in group velocity with higher l/h suggests that

nonlocality introduces additional wave dispersion, which is crucial for seismic wave analysis in nanostructures. The smooth, consistent curves validate the model's ability to handle bidirectional FGM while accounting for nonlocal and strain gradient effects. This figure underscores the importance of considering both material heterogeneity and nanoscale physics in dynamic structural analysis. Figure 2(b) illustrates phase velocity variations with respect to the FG power index for different length scale parameters. The higher velocity range compared to Fig. 2 suggests a different structural configuration or boundary condition. The results show a consistent decline in phase velocity with increasing FG power index, reinforcing the impact of material gradation on wave speed. Nonlocal effects further suppress phase velocity, demonstrating their damping influence. The HHSDT model accurately predicts these trends, confirming its ability to handle complex material distributions and nanoscale effects. The nonlinearity in the curves at lower FG power index values indicates strong sensitivity to length scale interactions, which is critical for high-frequency wave propagation. This figure highlights the necessity of advanced theoretical frameworks, such as q-3DHT, for precise seismic response predictions in nanostructures. Figure 2(c) illustrates the ratio of group velocity to phase velocity (0.38–0.54) as a function of $n_x = n_y = n_z$. The results show a gradual decline in the ratio with increasing $n_x = n_y = n_z$, indicating enhanced dispersion in steeper material gradients. The HHSDT model accurately predicts this behavior, demonstrating its capability to analyze wave energy transmission in functionally graded nanostructures. The figure provides valuable insights into the role of material gradation in modulating wave dispersion, which is critical for seismic engineering applications.

Figure 3(a) examines group velocity (1 000–3 500 m/s) as a function of the FG power index for varying nonlocal parameters. The results show that a higher FG power index and μ/h reduce group velocity, indicating slower energy propagation in steeper material gradients and stronger nonlocal interactions. The nonlinear behavior at a low FG power index suggests dominant nonlocal effects, while the smoother decline at higher values reflects material gradation's influence. The HHSDT model successfully predicts these trends, confirming its robustness in analyzing wave energy transmission in nanostructures. The findings are particularly relevant for seismic engineering, where accurate group velocity predictions are essential for understanding wave attenuation and energy dissipation in advanced materials. Figure 3(b) presents the relationship between maximum velocity and the power index for different nonlocal parameters ($\mu = 0.05, 0.1, 0.15$) in functionally graded nanostructures. The results demonstrate several key trends regarding wave propagation characteristics in these advanced materials. The data shows that maximum velocity decreases significantly with increasing nonlocal parameter μ, with values ranging from approximately 3 500 m/s at $\mu = 0.05$–2 000 m/s at $\mu = 0.15$

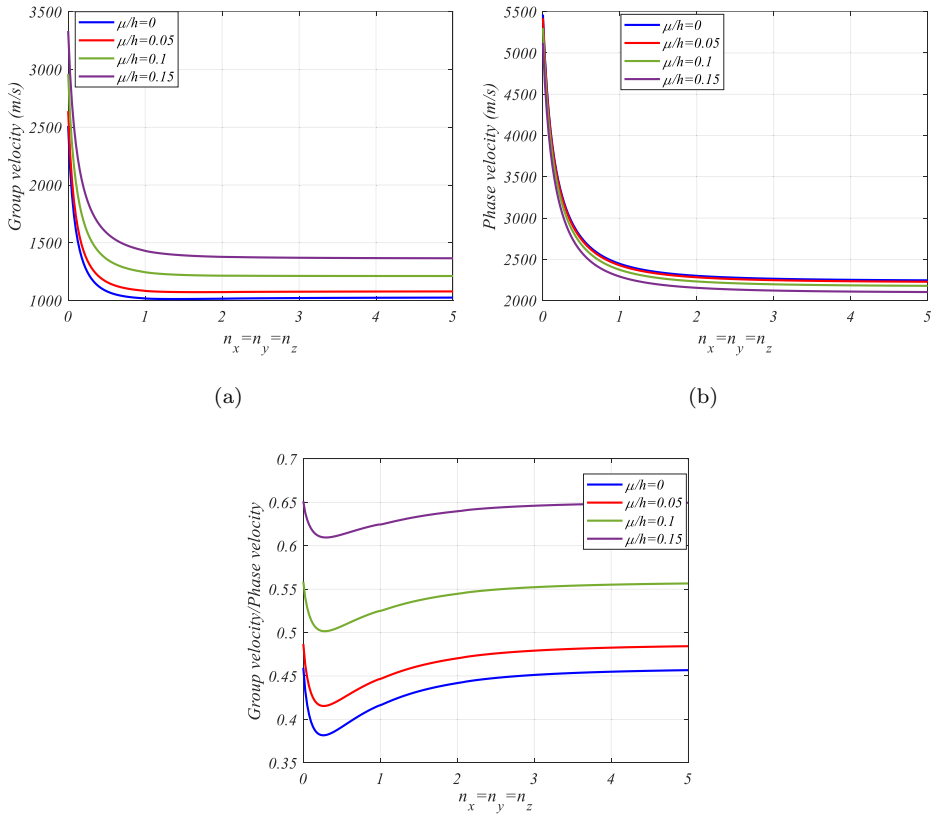

Fig. 3. The wave propagation characteristic as a function of the power index $n_x = n_y = n_z$ for different dimensionless nonlocal parameters.

when $n_x = n_y = n_z = 0$. This reduction in wave velocity highlights the substantial influence of nonlocal effects on dynamic behavior, where stronger nonlocality (higher μ) corresponds to greater wave attenuation and dispersion. The trend is consistent across all power index values, indicating that nonlocal effects remain dominant regardless of material gradation. Furthermore, the figure reveals that increasing the power index ($n_x = n_y = n_z$) from 0 to 5 leads to a gradual decrease in maximum velocity for each μ value. This suggests that material property gradation, represented by the power index, interacts with nonlocal effects to modify wave propagation characteristics. The most pronounced velocity reduction occurs at lower power indices ($0 < n_x = n_y = n_z < 1$), with the curve flattening at higher values. These findings have important implications for the design of functionally graded nanomaterials in seismic applications. The combined effects of nonlocality

and material gradation must be carefully considered when predicting wave propagation behavior, particularly for high-frequency vibrations where these factors significantly influence energy transmission and dissipation. The results underscore the need for advanced theoretical models, such as the HHSDT, that can accurately capture these complex interactions in nanostructured materials. The smooth, well-defined curves in the figure validate the robustness of the computational approach, providing reliable data for engineering applications where precise control of wave propagation is required. This analysis contributes to the fundamental understanding of wave mechanics in functionally graded nanostructures, offering valuable insights for material design and optimization in seismic-resistant applications. Figure 3(c) presents the ratio of group velocity to phase velocity against FG power index for different μ/h values. The decreasing ratio with increasing FG power index indicates greater wave dispersion in strongly graded materials. Nonlocal effects ($\mu/h > 0$) further reduce the ratio, highlighting their damping role in wave energy transmission. The HHSDT model accurately captures these trends, demonstrating its effectiveness in predicting dynamic responses in 3D-FGM nanostructures. The results emphasize the importance of considering both material gradation and nanoscale effects in seismic wave analysis. This figure provides critical insights for designing nanostructures with controlled wave dispersion and energy dissipation properties.

Figure 4(a) depicts group velocity (1 000–8 000 m/s) as a function of wave number for different length scale parameters ($\frac{l}{h} = 0, 0.005, 0.01, 0.015$). The results show that higher l/h values increase group velocity, reflecting the stiffening effect of strain gradients. The HHSDT model effectively reconciles these trends with nonlocal effects, providing a comprehensive understanding of wave dynamics in 3D-FGM nanostructures. The figure highlights the model's accuracy in predicting high-frequency wave responses, which is essential for seismic-resistant material design. Figure 4(b) depicts phase velocity (2 000–16 000 m/s) as a function of wave number (0–100 1/nm) for different l/h values. Unlike nonlocal effects, higher l/h increases phase velocity, indicating a stiffening effect due to strain gradients. The HHSDT model reconciles these competing mechanisms (nonlocal softening versus strain gradient hardening), providing a comprehensive understanding of wave propagation in 3D-FGM nanostructures. The results highlight the model's ability to predict high-frequency wave responses accurately, which is crucial for seismic applications. The figure underscores the necessity of advanced theoretical approaches in analyzing nanostructures under dynamic loading conditions. Figure 4(c) plots the ratio of group velocity to phase velocity against wave number (0–100 1/nm) for different dimensionless length scale parameters ($\frac{l}{h} = 0, 0.005, 0.01, 0.015$). The decreasing trend in the ratio with increasing wave number confirms strong wave dispersion. Higher l/h values reduce the ratio, emphasizing the role of strain gradient effects in wave energy transmission. The HHSDT model effectively captures these dispersion

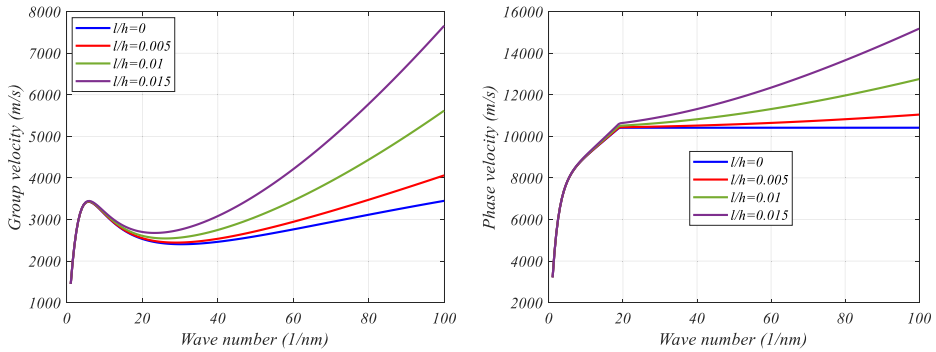

(a)

(b)

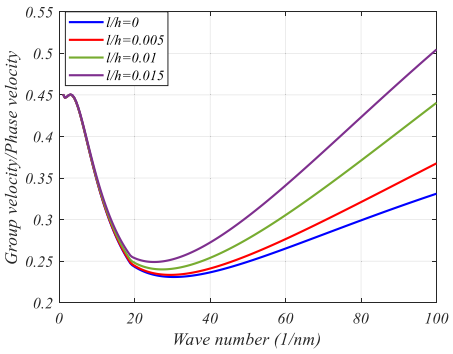

(c)

Fig. 4. The wave propagation characteristic as a function of the wave number for different dimensionless length scale parameters.

characteristics, demonstrating its capability to model high-frequency wave behavior in 3D-FGM nanostructures. The results suggest that microscale interactions significantly influence wave propagation, particularly in seismic applications where dispersion effects are critical. The figure validates the model's accuracy in predicting dynamic responses, making it a valuable tool for nanoengineered material design.

Figure 5(a) presents group velocity variations with respect to wave number for different nonlocal parameters. The results show that higher μ/h values reduce group velocity, indicating slower energy propagation due to nonlocal interactions. The HHSDT model accurately predicts these trends, confirming its ability to handle nanoscale effects in wave dynamics. The figure underscores the significance of nonlocality in modulating wave energy transmission, particularly in seismic-resistant nanomaterials. The smooth, consistent curves validate the model's robustness in analyzing complex wave behaviors under varying material and scale conditions.

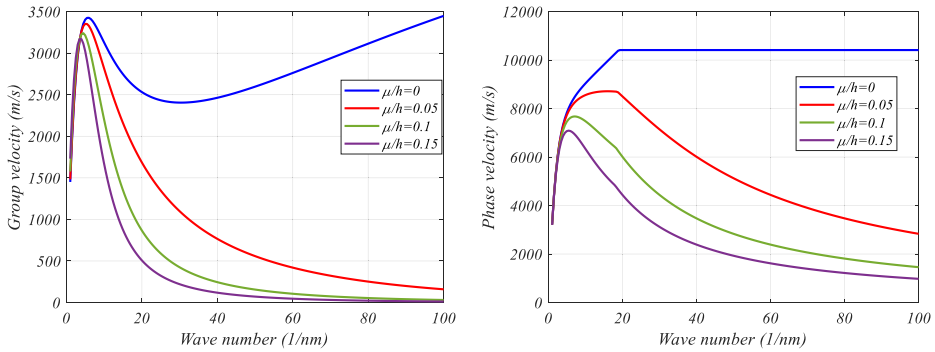

(a)

(b)

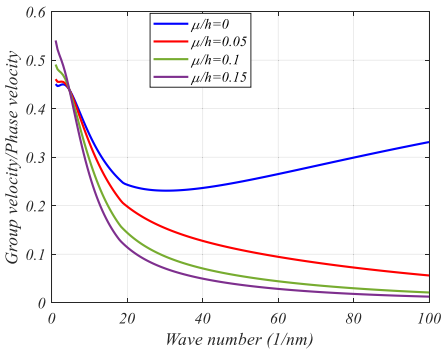

(c)

Fig. 5. The wave propagation characteristic as a function of the wave number for different dimensionless nonlocal parameters.

Figure 5(b) depicts phase velocity (0–12 000 m/s) as a function of wave number for different μ/h values. The results reveal that nonlocal effects significantly reduce phase velocity, demonstrating their softening influence on wave propagation. The HHSDT model effectively reconciles these effects with material gradation, providing a comprehensive understanding of wave dynamics in 3D-FGM nanostructures. The figure highlights the model's accuracy in predicting high-frequency wave responses, which is essential for seismic engineering applications. The findings emphasize the need for advanced theoretical frameworks to capture nanoscale interactions in dynamic analyses. Figure 5(c) illustrates the ratio of group velocity to phase velocity (0.1–0.6) as a function of wave number for different nonlocal parameters ($\frac{\mu}{h} = 0, 0.05, 0.1, 0.15$). The decreasing trend in the ratio with increasing wave number indicates strong wave dispersion, particularly at higher frequencies. Nonlocal effects further reduce the ratio, demonstrating their

damping influence on wave energy transmission. The HHSDT model effectively captures these dispersion characteristics, highlighting its capability to predict dynamic responses in 3D-FGM nanostructures. The results emphasize the importance of considering nonlocal interactions in high-frequency wave propagation, which is critical for seismic applications. This figure provides valuable insights into the interplay between material properties and nanoscale effects on wave dispersion.

5. Conclusion

This study has investigated the nonlinear dynamic stability and phase/group velocity characteristics of waves in three-dimensional functionally graded skew nanoplates, specifically for concrete building applications. A HHSDT has been employed to model the structural behavior, accounting for von-Karman geometrical nonlinearity to capture large deformations, while the NSGT has been integrated to address nanoscale effects. The governing equations of motion have been derived using Hamilton's principle and have been solved numerically through an advanced finite element method, where isoparametric elements have been converted to standard elements to optimize computational stability and accuracy. Due to the nonlinear nature of the system, an efficient iterative solution strategy has been developed and validated. This study has investigated the nonlinear dynamic behavior and wave propagation characteristics of waves in functionally graded skew nanoplates. Key findings have shown that material gradation, nonlocal effects, and nanoscale interactions have significantly influenced phase and group velocities, particularly at higher frequencies. The HHSDT model has provided superior accuracy over traditional models in predicting wave behavior in such materials. These insights have proven crucial for seismic engineering, structural health monitoring, and nondestructive testing. Future research could explore multi-field coupling effects, temperature dependence, and anisotropy, further advancing nanostructure design for optimized dynamic performance in engineering applications. Here are five highlights based on the current results:

(1) Material gradation decreases both phase and group velocities, especially with higher FG power indices.
(2) Nonlocal effects significantly reduce phase and group velocities, emphasizing the impact of nanoscale interactions.
(3) Lower FG power indices show greater sensitivity of phase velocity to material gradation and nonlocal effects.
(4) Group and phase velocity ratios decrease as the FG power index increases, indicating enhanced wave dispersion.

(5) Higher μ/h values lead to slower energy propagation, highlighting the influence of nonlocal interactions on waves.

Acknowledgment

The authors extend their appreciation to King Saud University, Saudi Arabia, for funding this work through the Ongoing Research Funding Program, (ORF-2025-993), the King Saud University, Riyadh, Saudi Arabia.

References

1. M. Abasi, K. Arshadi, M. Rafiei and H. Afshari, The aeroelastic stability characteristics of a ring-stiffened conical three-layered sandwich shell with an FG auxetic honeycomb core utilizing zig-zag shell theory, *Aerosp. Sci. Technol.* **155** (2024) 109551.
2. M. Al-Furjan, S. Fan, L. Shan, A. Farrokhian, X. Shen and R. Kolahchi, Wave propagation analysis of micro air vehicle wings with honeycomb core covered by porous FGM and nanocomposite magnetostrictive layers, *Waves Random Complex Media* (2023) 1–30.
3. S. Al-Houri, M.A. Al-Osta, Q. Gawah, F. Bourada, A. Tounsi, S. U. Al-Dulaijan and A. Tounsi, Wave propagation analysis of composite beams reinforced with nonlinear FG-CNT distributions supported on Kerr elastic foundation utilizing an improved integral first-order shear deformation theory, *Geomech. Eng.* **39** (2024) 483.
4. A. G. Arani, R. Kolahchi, A. M. Barzoki and A. Loghman, Electro-thermo-mechanical behaviors of FGPM spheres using analytical method and ANSYS software, *Appl. Math. Model.* **36** (2012) 139–157.
5. M. Arefi, E. Mohammad-Rezaei Bidgoli and A. M. Zenkour, Free vibration analysis of a sandwich nano-plate including FG core and piezoelectric face-sheets by considering neutral surface, *Mech. Adv. Mater. Struct.* **26** (2019) 741–752.
6. B. Deng, J. R. Raney, K. Bertoldi and V. Tournat, Nonlinear waves in flexible mechanical metamaterials, *J. Appl. Phys.* **130** (2021) 040901.
7. S. P. Wallen, W. DeLima and M. R. Haberman, Strongly nonlinear wave propagation in elasto-plastic metamaterials: Low-order dynamic modeling, *J. Mech. Phys. Solids* **204** (2025) 106276.
8. M. M. Khater, S. H. Alfalqi, J. F. Alzaidi and R. A. Attia, Analytically and numerically, dispersive, weakly nonlinear wave packets are presented in a quasi-monochromatic medium, *Results Phys.* **46** (2023) 106312.
9. L. Chang, Y. Hu and A. E. Ragab, On the nonlinear wave propagations of improved solar cells, *Aerosp. Sci. Technol.* **146** (2024) 108941.
10. L. Chang, H. Wu, Y. Hu and A. M. El-Sherbeeny, Nonlinear elastic wave dispersions of solar cells strengthened by advanced functionally graded materials via both mathematical modeling and deep neural networks technique, *Aerosp. Sci. Technol.* **147** (2024) 109010.
11. Y. Ni, S. Zhu, Z. Tong, X. Xu, Z. Zhou, C. Lim, M. Ahmer Wadee and S. Yiatros, Stability of composite cylindrical shells with nonclassical hygrothermal–electro–elastic coupled loads, *J. Eng. Mech.* **149** (2023) 04022113.
12. V. H. Nam, N.-T. Trung, N. T. Phuong, V. M. Duc and V. T. Hung, Nonlinear torsional buckling of functionally graded carbon nanotube orthogonally reinforced

composite cylindrical shells in thermal environment, *Int. J. Appl. Mech.* **12** (2020) 2050072.
13. H. M. Hasan, S. S. Alkhfaji and S. A. Mutlag, Torsional postbuckling characteristics of functionally graded graphene enhanced laminated truncated conical shell with temperature dependent material properties, *Theor. Appl. Mech. Lett.* **13** (2023) 100453.
14. A. Y. Ali, H. M. Hasan and F. M. Mohammed, Nonlinear dynamic buckling of a simply supported imperfect nanocomposite shear deformable plate under the effect of in-plane velocities, *Commun. Nonlinear Sci. Numer. Simul.* **138** (2024) 108232.
15. B. Farahmand-Azar, G. Pourmoosavi and S. Talatahari, Sound transmission loss analysis of double-walled sandwich functionally graded carbon nanotube-reinforced composite magneto-electro-elastic plates under thermal environment, *J. Vib. Control* **30** (2024) 4551–4571.
16. M. Eroğlu, I. Esen and M. A. Koç, The effect of an auxetic core layer and symmetric FGM face layers on the 3D wave propagation response of sandwich nanoplates, *Arch. Appl. Mech.* **95** (2025) 69.
17. M. Janghorban and A. Tounsi, Two models for wave propagation in polymer/halloysite nanotube nanocomposites: Network phenomena/generalized continuum mechanics, *Waves Random Complex Media* (2024) 1–32.
18. C. Liu, J. Yu, B. Zhang and C. Zhang, Size parameter calibration of nonlocal strain gradient theory based on molecular dynamics simulation of guided wave propagation in aluminum plates, *Thin-Walled Struct.* **198** (2024) 111659.
19. P. R. Saffari, C. Thongchom, P. R. Saffari, J. Lawongkerd, S. Keawsawasvong and T. Senjuntichai, Free vibration of thermally loaded FG-GPLRC nanoplates integrated with magneto-electro-elastic layers in contact with fluid, *Int. J. Struct. Stab. Dyn.* **25** (2025) 2550113.
20. Z. Jalali-Mola, S. Asgarnezhad-Zorgabad and O. Hess, Collective quantum dynamics with distant quantum emitters in slow-wave nanoplasmonic waveguides, *APL Quantum* **1** (2024) 046104.
21. S. Han, Q. Ye, H. A. Mahmoud and A. Elbarbary, Nonlinear phase velocities in tri-directional functionally graded nanoplates coupled with NEMS patch using multi-physics simulation, *Aerosp. Sci. Technol.* **156** (2025) 109714, doi:10.1016/j.ast.2024.109714.
22. C. Krishnaveni and S. S. Selvan, Study on nano-alumina in concrete, *Mater. Today. Proc.* **46** (2021) 3648–3652.
23. H. Behbahani, B. Nematollahi and M. Farasatpour, Steel fiber reinforced concrete: A review, in *Proc. Int. Conf. Structural Engineering Management and Construction* (ICSECM, Kandy-SriLanka, 2011), pp. 1–12.
24. P. Van Vinh and L. Q. Huy, Finite element analysis of functionally graded sandwich plates with porosity via a new hyperbolic shear deformation theory, *Def. Technol.* **18** (2022) 490–508, doi:10.1016/j.dt.2021.03.006.
25. J. N. Reddy, *Mechanics of Laminated Composite Plates and Shells: Theory and Analysis* (CRC Press, 2003).
26. G.-L. She, Z.-S. Ma, C. Li and M. A. Eltaher, Geometrically nonlinear transient response of graphene platelets reinforced metal foams arbitrary quadrilateral plates under blast load, *Thin-Walled Struct.* **210** (2025) 113018, doi:10.1016/j.tws.2025.113018.
27. J. Achenbach, *Wave Propagation in Elastic Solids* (Elsevier, 2012).

28. B. Karami and M. H. Ghayesh, Wave propagation characteristics of quasi-3D graphene origami-enabled auxetic metamaterial plates, *Int. J. Eng. Sci.* **207** (2025) 104185, doi:10.1016/j.ijengsci.2024.104185.
29. H. Aminipour and M. Janghorban, Wave propagation in anisotropic plates using trigonometric shear deformation theory, *Mech. Adv. Mater. Struct.* **24** (2017) 1135–1144, doi:10.1080/15376494.2016.1227500.
30. M. R. Nami and M. Janghorban, Wave propagation in rectangular nanoplates based on strain gradient theory with one gradient parameter with considering initial stress, *Mod. Phys. Lett. B* **28** (2014) 1450021.
31. S. I. Tahir, A. Tounsi, A. Chikh, M. A. Al-Osta, S. U. Al-Dulaijan and M. M. Al-Zahrani, An integral four-variable hyperbolic HSDT for the wave propagation investigation of a ceramic-metal FGM plate with various porosity distributions resting on a viscoelastic foundation, *Waves Random Complex Media* **34** (2021) 1–24, doi:10.1080/17455030.2021.1942310.